Applications of Artificial Intelligence on Thermal Imaging

Chapter · July 2020

CITATIONS
0

READS
307

3 authors:

Saim Ervural
Karatay Univeristy
14 PUBLICATIONS **17** CITATIONS
SEE PROFILE

Ahmet Haydar Ornek
Konya Technical University
12 PUBLICATIONS **17** CITATIONS
SEE PROFILE

Murat Ceylan
Konya Technical University
78 PUBLICATIONS **435** CITATIONS
SEE PROFILE

CLASSIFICATION OF UNHEALTHY AND HEALTHY NEONATES IN NEONATAL INTENSIVE CARE UNITS USING MEDICAL THERMOGRAPHY PROCESSING AND ARTIFICIAL NEURAL NETWORK

Duygu Savasci[1], Ahmet Haydar Ornek[1], Saim Ervural[2]
Murat Ceylan[1], Murat Konak[3], Hanifi Soylu[3]

[1] Faculty of Engineering Electrical-Electronic Engineering Dept.
Selcuk University, Konya
duyguzn8559@gmail.com, ahmethaydarornek@gmail.com, mceylan@selcuk.edu.tr

[2] Faculty of Engineering, Electrical-Electronic Engineering Dept.
KTO Karatay University, Konya
saim.ervural@karatay.edu.tr

[3] Faculty of Medicine, Division of Neonatology, Department of Pediatrics
Selcuk University, Konya
drmkonak@hotmail.com, hasoylu@hotmail.com

ABSTRACT

Tracking of the temperature changes for the neonatal being in the neonatal intensive care unit is quite important in the pre-diagnosis of diseases or the evaluation of follow-up treatment. The purpose of this study is to develop an analysis system based on thermal imaging, which is the contact-free, non-ionized and non-invasive method for the neonatal. For this purpose, 190 images taken from 19 healthy and 19 unhealthy neonates were used. In general, this study consists of three steps. Firstly, the temperature map of the images was segmented. Then, Discrete Wavelet Transform (DWT), Curvelet Transform (CuT) and Contourlet Transform (CoT) as multi-resolution methods were applied to them and feature vectors were extracted by using their approximate coefficients. After that, all feature vectors were given as an input to the artificial neural network. According to the results obtained, the best accuracy rate was 98.42% when using DWT.

Keywords: Neonatal, Infrared Thermography, Medical Thermography Processing, Multi-resolution Analysis, Artificial Neural Network.

1 Introduction

All objects being above absolute zero (-273,15°C, 0K) emit infrared radiation, depending on their temperature and their spectral emissivity [1]. The amount of radiation emitted by the body is in the infrared area of the electromagnetic spectrum and the wavelength is in the range of 0.75-1000 micrometers [2]. Skin emissivity is a significant element for determining skin temperature and is valued at 0-1, depending on the wavelength [3]. The emissivity of human skin is between 0.96-0.98. It behaves nearly like a blackbody [4]. The blackbody is accepted as an object absorbing all incoming energy and emitting energy continuously according to the Planck's law [5]. The energy emitted by a blackbody is at the maximum value for a given temperature [1]. Therefore, since the emissivity of human skin is close to the emissivity of a blackbody, the infrared radiation emitted by the skin can be directly converted into temperature values by using thermal imaging.

Thermal images is used for measure the distribution of temperature organs and tissues by capturing the infrared radiation. Thermal imaging can be used on a variety of conditions to plan treatment, evaluate its effects and examine physiological functions in healthy people [2]. Temperature changes caused by physiological disorders can be detected without giving any discomfort and radiation damage to the patient. Physiological function disorders that occur in the body cause temperature increases. These increments are shown as hot spots or asymmetrical patterns on the infrared images. Distribution of the skin temperature of a normal human body shows contralateral symmetry. Temperature distribution with asymmetry above a certain level is usually a reliable indicator of abnormalities [6]. Therefore, since the healthy body is thermally symmetrical, asymmetric temperatures can be easily recognized on images.

Thermal camera converts infrared energy into electronic signals. These signals match the temperature values and can be displayed as an image on the screen [7]. This image is called as a thermogram. The temperature values of the thermograms can be visually displayed in gray level or in different color palettes. Thermograms become images as pixels arranged in a two-dimensional array [8]. Each pixel represents the temperature values of the displayed region [2].

Thermal cameras used in medical applications usually operate at medium wave infrared (MWIR) wavelengths of 3 - 5 μm and long wave infrared wavelengths of 8 - 13 μm [1]. The choice of the type of the camera to be used is related to the temperature range of the objects to be examined [9]. The infrared radiation emitted by the human body has a wavelength of 8-12 μm that's why long-wave thermal cameras are generally preferred in thermal imaging.

In recent years, studies on neonatal intensive care units of thermal imaging methods, which have increased in effectiveness in medical applications, have become widespread because the importance of thermal imaging which is a non-contact, non-ionizing, non-invasive and harmless method for intensive care units has been noticed [10].

Temperature is one of the accepted sign of the structural health of components. So, analysis of body temperature of infants in the neonatal intensive care unit is important. The assessment of body temperature changes ensures that vital decisions are made, such as the need for immediate intervention, new treatment planning or stabilization. Computerized Tomography (CT) and Magnetic Resonance (MR) imaging are frequently used for diagnostic purposes in neonatal infants nowadays; however, these techniques may not be suitable for neonates for three reasons. Firstly, physically disadvantaged neonates often go to the radiology department and are exposed to long-lasting images, which can cause a drop in the body temperature of these neonates. Unfortunately, the falling in these neonates' body temperatures causes hypothermia. Secondly, neonates are exposed to radiation during CT. Finally, it is almost impossible for neonates attached to the respiratory support device to be taken to the radiology department. By using thermal imaging, it is possible to detect the disease early and monitor the treatment period without any radiation and surgical treatment to neonates in intensive care unit. The purpose of this work is to create an analysis system based on thermal imaging for neonatal intensive care units.

2 Methods

The images captured by the thermal camera were segmented and by applying multiresolution analysis methods on segmented images, features were extracted. Then, these features were given as an input to the ANN and the images were classified as unhealthy or healthy. A block diagram of the system is illustrated in Figure 2.1.

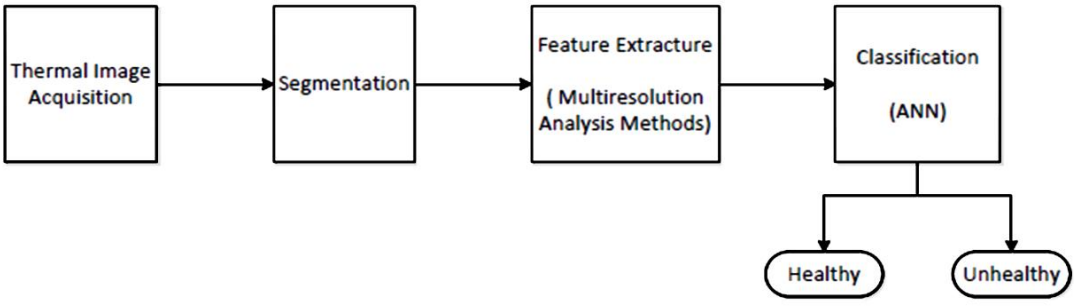

Fig. 2.1 Block diagram of the proposed system

The methods used in the study includes three sections. Firstly, the segmentation part is explained in Sect. 2.1. Secondly, multiresolution analysis methods which are used for feature extraction are described in Sects. 2.2. Finally, the method used in the classification part is presented in Sect. 2.3. In addition to these three sections, the performance evaluation procedures of the proposed system are described in Sect. 2.4.

2.1 Segmentation

Every newborn has different conditions and body temperature. For example, while some incubators are open, some incubators are heated from the outside with an external heater. However, background temperatures and body temperature values are different at the same time. For this reason, an algorithm is used to 'background subtraction', and the system automatically generates a threshold value. Figure 2.2 (a) displays the neonatal image by visualizing the temperature map, Figure 2.2 (b) shows the temperature map with threshold value algorithm applied, and Figure 2.3 illustrates the steps of segmentation.

Fig. 2.2 (a) Visualization of temperature map (b) Temperature map image after using a threshold algorithm

As seen in Figure 2.2, some newborns lying in the incubator have latches attached to their navel. For those objects that are cold relative to the body, black areas appear on the part where the latch is located, as shown in Figure 2.2 (b). A gap filling algorithm was used to fill these black areas within body boundaries. Figure 2.4 shows the resulting image after applying the gap filling algorithm.

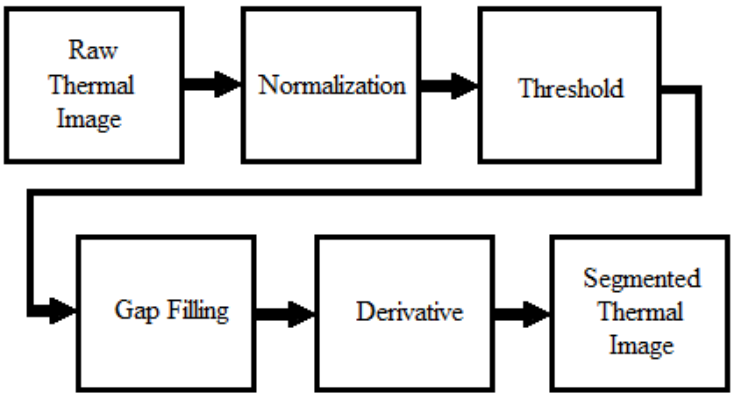

Fig 2.3 Steps of segmentation process

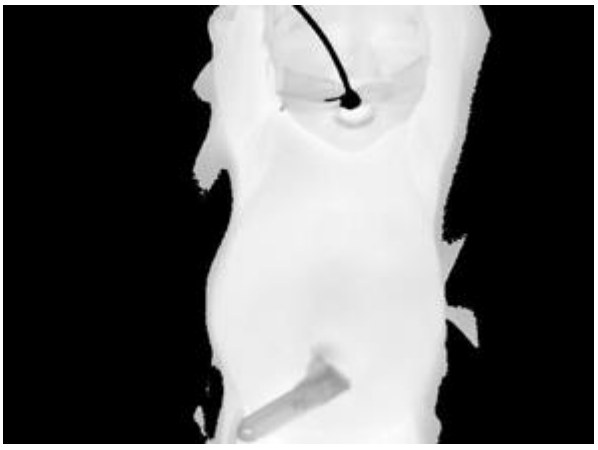

Fig 2.4 Temperature map image after using hole filling algorithm.

After the threshold value and gap filling algorithms have been completed, to observing the change in temperature, took the derivative of image (1). For this operation, the temperature value f(x) in all the rows has been subtracted from the previous temperature value f(x-1)

$$\frac{df}{dx} = f(x) - f(x-1) \quad (1)$$

Thus, a matrix containing temperature changes is obtained. As shown in Figure 2.5, this matrix has positive and negative values. To binarizing this matrix, zero or less than zero values equalized to 0 and greater than zero values equalized to 1. Figure 2.6 shows the binary matrix and visualizing the binary matrix.

-0.08	-0.08	-0.04	-0.1	-0.09	-0.05
0.02	-0.04	0.02	0.03	0.03	0.02
-0.08	0.03	-0.02	-0.03	-0.05	-0.02
-0.01	-0.06	-0.04	-0.02	-0.02	-0.06
-0.02	0	-0.03	-0.01	0.02	0.03
-0.01	-0.07	-0.1	-0.02	0.02	0.02
0.07	0.03	-0.03	-0.05	-0.04	-0.08
-0.04	0.03	0.08	0.01	-0.04	-0.02
0.01	-0.05	-0.04	-0.01	-0.04	-0.08
-0.03	0	-0.03	-0.05	-0.01	0.01
-0.04	-0.05	0.02	0.04	0.05	0.09
0.04	-0.02	-0.02	0.01	0	-0.01
0	0.01	0.06	0.02	-0.02	-0.03
0.03	0.03	0.01	0.08	0.1	0.09
0.11	0.16	0.16	0.12	0.11	0.11

Fig 2.5 Matrix representation of temperature changes

0	0	0	0	0	0
1	0	1	1	1	1
0	1	0	0	0	0
0	0	0	0	0	0
0	0	0	0	1	1
0	0	0	0	1	1
1	1	0	0	0	0
0	1	1	1	0	0
1	0	0	0	0	0
0	0	0	0	0	1
0	0	1	1	1	1
1	0	0	1	0	0
0	1	1	1	0	0
1	1	1	1	1	1
1	1	1	1	1	1

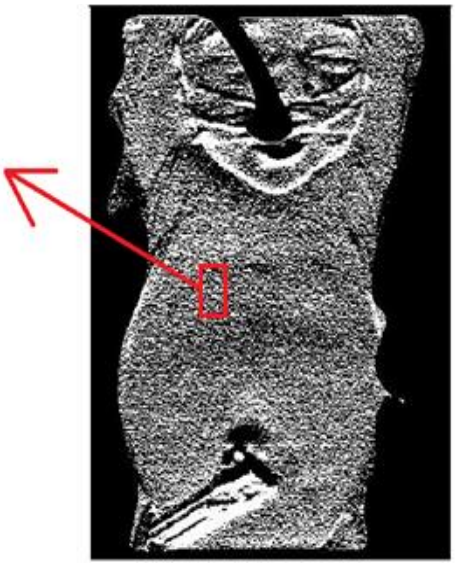

Fig 2.6 Binary matrix and visualizing the binary matrix

2.2 Multiresolution Analysis Methods

Multiresolution analysis (MRA) is used to extract the desired information from the image. So, multiresolution analysis can be used for various image processing applications such as image segmentation, wavelet-based features, image compression, denormalization and classification.

The basis of the multiresolution analysis methods is Wavelet Transform (WT). While the continuous form of the Wavelet Transform was presented by Morlet (1982) [11], the discrete form of the Wavelet Transform was developed by Mallat (1989) [12] and Daubechies (1992) [13].

Wavelet transform allows analyzing images in lower frequency bands. Wavelet Transform divides the image into a series of high-pass and low-pass filter bands to extract directional details that capture horizontal, vertical, and diagonal-activity. [14]. Thus, Wavelet Transformation can only acquire limited information due to the weakness of the choice of orientation. Wavelet Transform can not effectively represent objects with highly anisotropic elements, such as lines or curved structures, because they can not take advantage of the edge curve's regularity [15]. To remove these problems, some new methods were developed. These methods cover Curvelet Transform (CuT), which allows continuous linear information to be extracted more flexible with curvilinear windowing, was developed by Candes and Donoho (2000) [16], and Contourlet Transform (CoT), which emphasizes border information, was laid by Do and Vetterli (2005) [17]. These methods will be explained in detail in the following parts.

2.2.1 2D Wavelet Transform

The Wavelet Transform extracts features of the image by performing shifting or scaling operations. Wavelet coefficients with different directions and scales are obtained [18]. Calculating DD coefficients for every shifting and scaling causes a lot of and unused data to produce. Evaluating scale and shift parameters of Wavelet Transform in discrete time-scale domain results in creating Discrete Wavelet Transform (DWT). So, in DWT, the scale and shift parameters are represented in a discrete time-scale domain. DWT enables the efficient use of resources by reducing the calculation time of the time and frequency information of the image to a large extent [19] [20].

The outputs of a first-order high-pass filter and low pass filter are cD1 and cAl, respectively, which are shown in Figure 2.7. The signal is divided into the desired frequency range by repeating this operation for more than one level successively. While approximation coefficients, which show low-frequency components, are obtained from low pass filters, detail coefficients, which illustrate high-frequency components, are achieved from high pass filters. Properties of signal keep on approximation coefficients, and the process can be continued gradually through these coefficients [21].

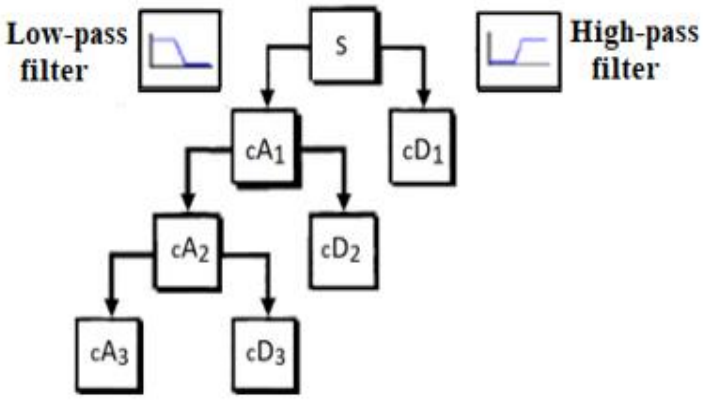

Fig 2.7 The filter bank for Discrete Wavelet Transform

For images, one-dimensional Discrete Wavelet Transform (1D-DWT) can be easily extended into two dimensional (2D). Two-dimensional Discrete Wavelet Transform (2D-DWT) was achieved by applying the 1D-DWT to the rows and columns of the image separately. Three details (HL, LH, HH) and one approach (LL) components are produced horizontal, vertical and diagonal with 2D-DWT. Multi-level decomposition can be performed by decomposing the approximation component multiple times in the same way as a dimensional discrete transformation as shown in figure 2.8 [21]. Figure 2.9 shows an approximation component of the transform coefficient obtained by applying DWT on the image which was used in the study.

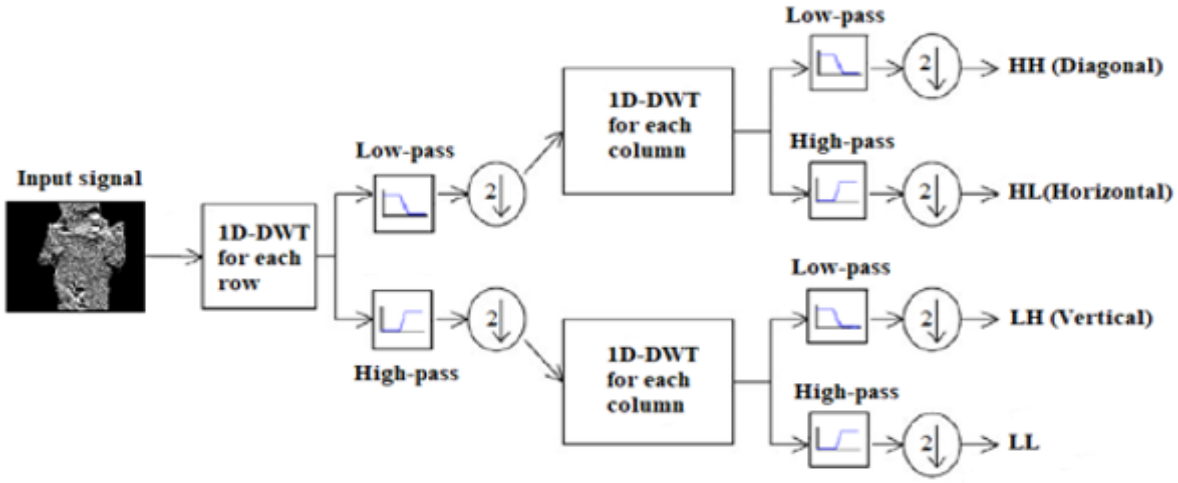

Fig 2.8 2D-DWT filter structure for image analysis

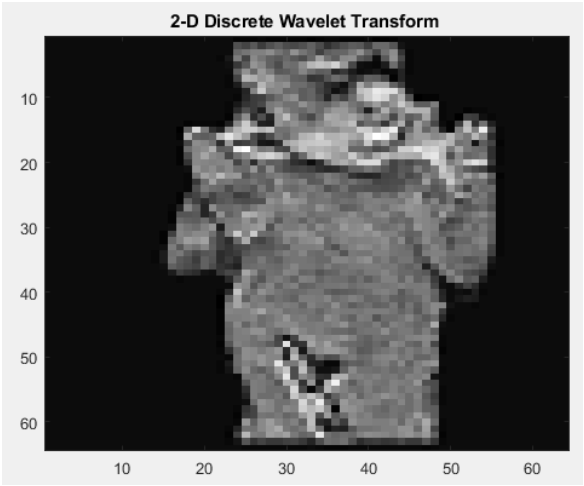

Fig 2.9 Display of approximation coefficients obtained by applying DWT on the image

2.2.2 2D Curvelet Transform

Curvelet Transform has been introduced as a new Wavelet Transform that is suitable for finding edge regions in 2D images. Since the Wavelet Transform does not benefit from the geometry of the edge curve, wavelets can not effectively represent objects with edges. [15].

The Curvelet Transformation is designed to represent edges and other singularities along curves using fewer coefficients. The Curvelet Transform consists of a multi-scale pyramid with many orientations and positions at each length scale [22]. Curvelets are basic elements that exhibit very high directional accuracy and are highly anisotropic. They have good orientation features due to the structural elements of the Curvelet Transform, including size, position and orientation parameters. [23].

Curvelet Transform is designed based on Ridgelet Transform. On the contrary Wavelet Transform and Ridgelet Transform, curvilinear windows are defined instead of linear windows in Curvelet Transform. Thus, the images are made sense of with less distortion by increasing intersection areas of them with the window.

The Curvelet Transformation is performed by dividing the original image into different scaled subbands and then by spatial partitioning each subbands. Then, for all scales, the Ridgelet Transformation is applied to each block. The main structure of the Ridgelet Transform consists of three basic transformations: Discrete Fourier transform, Radon transform, and Wavelet Transform. Ridgelet Transform is used in image processing applications to determine the singularities on the edges of the image. Radon Transform is a transform that allows two-dimensional image properties to be determined [15].

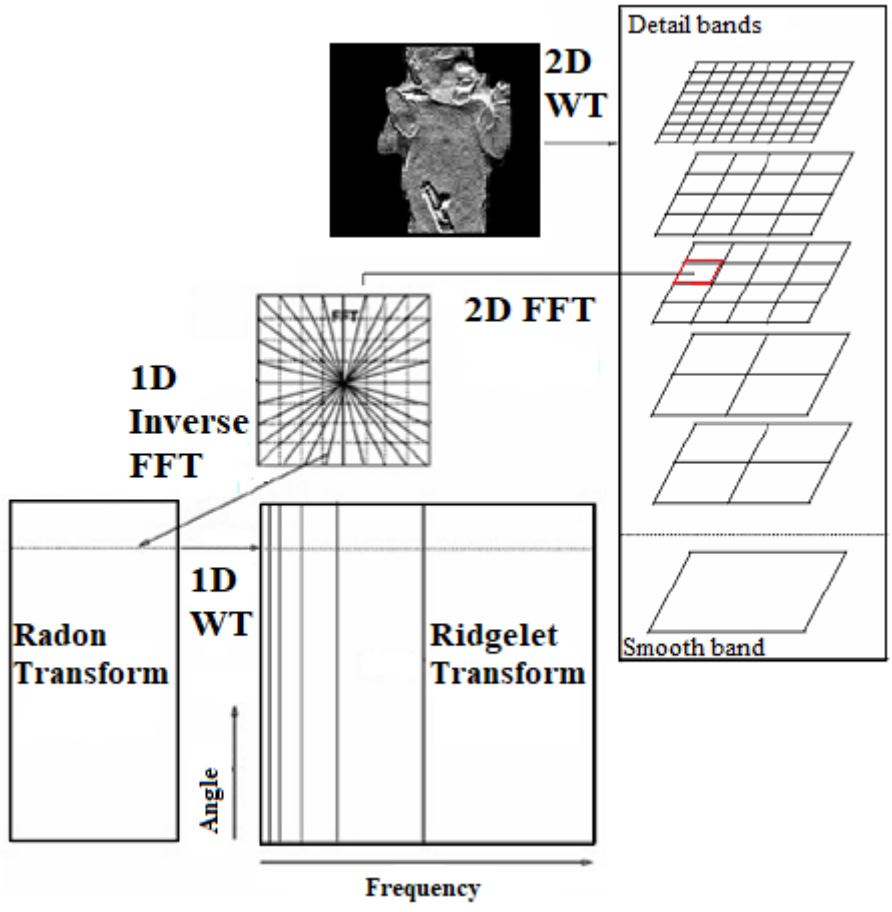

Fig 2.10 Scheme of the First-Generation Curvelet Transform

In the literature, the Curvelet Transform is processed under two generations. The First-Generation Curvelet Transform was introduced by Candes and Donoho (1990) [16]. Transform

is uses a series of steps including transformation, Ridgelet Analysis, and a Radon Transformation of an image. A scheme of the First-Generation Curvelet Transform is shown in Figure 2.10. Curvelet Transform's Second-Generation was suggested by Candes and Guo (2002), which is easier to understand and use. It was defined directly via frequency partitioning without using the ridgelet transform [24]. Later, the Fast Discrete Curvelet Transform (FDCT) based on Second-Generation Curvelet Transform was developed by Candes et al. (2006) [25]. Thus, FDCT can be implemented faster, less redundantly and simpler than First-Generation Curvelet Transform. FDCT can be implemented by either the Unequally Spaced Fast Fourier Transform (USFFT) or the Wrapping method. These two implementations are differed by spatial grid used to translate curvelets at each angle and scale. Both USFFT and Wrapping method digital return a table of numerical curvelet coefficients indexed by an orientation parameter, scale parameter and spatial location parameter [25]. In this study, the Curvelet Transform via Wrapping method was used. Figure 2.11 shows approximation coefficients obtained by applying the Curvelet Transform via Wrapping method on the image which was used in the study.

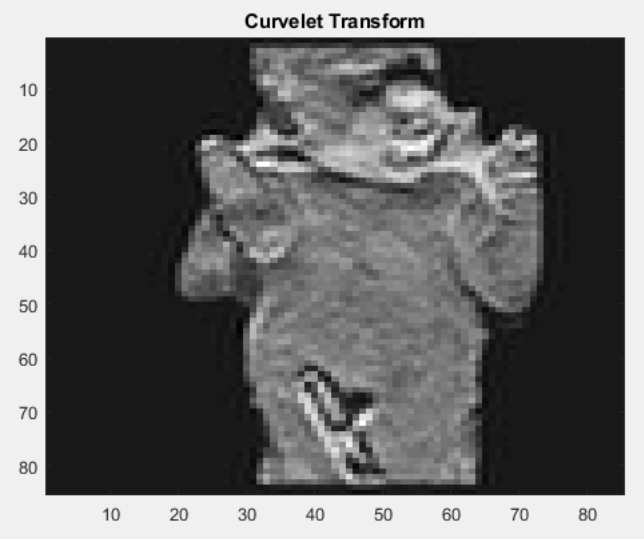

Fig 2.11 Display of approximation coefficients obtained by applying Curvelet Transform via Wrapping method on the image

2.2.3 2D Contourlet Transform

The fact that the Wavelet Transform can only get information in specific directions and the lack of certain continuity in obtaining information on the contour was caused the Contourlet Transform to emerge.

The main purpose of the Contourlet Transform is a discrete extension of fragmented soft images, lacking completely flat contours with high degree of anisotropy and versatility. The Contourlet Transform presents directionality and contour-capture characteristics. In addition, the multiscale also has some Wavelet features such as time, frequency and localization features. The most considerable benefit of this transform is that it improves the contours or smoothly delivers those contours that use fewer coefficients than those requested by Wavelets. [26].

Contourlet Transform consists of two main elements, which are Laplace analysis and directional filtering. The first operation in Contourlet is to apply Laplace analysis to take point discontinuities. The basic idea behind the Laplacian pyramid is to produce approaches such as low-pass filtering and downsampled for the signal. Then, Directional Filter Bank (DFB) are used to bind point discontinuities to a linear structure. The DFB is designed to grab the high-frequency components of the image. That is, DFB can not be analyze low frequencies. This method attempts to obtain the original signal. Numerous analysis and synthesis steps can be performed until near the original signal. The Contourlet Filter Bank is formed by the sequential use of Laplace analysis and Directional Filter Bank [17]. Contourlet Filter Bank structure is shown in Figure 2.12. Figure 2.13 is shown an approximation component of the transform coefficient obtained by applying Contourlet Transform on the image which was used in the studies.

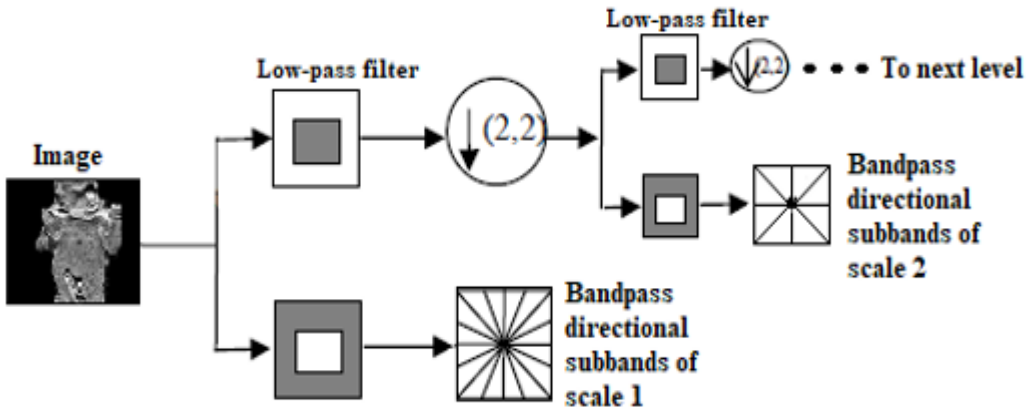

Fig. 2.12 Contourlet Filter Bank structure.

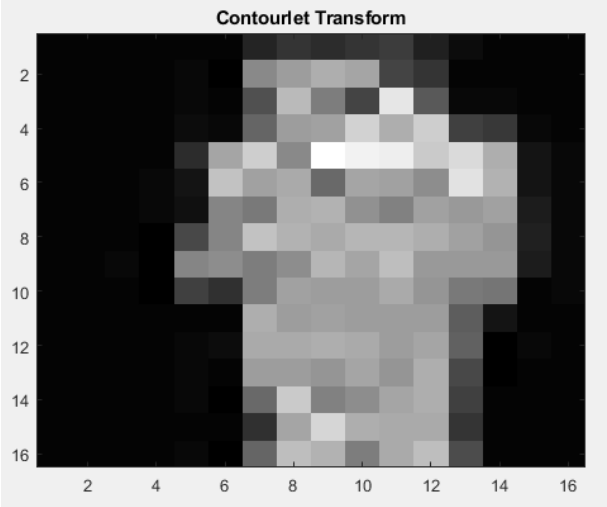

Fig. 2.13 Display of approximation coefficients obtained by applying Contourlet Transform on the image.

2.3 Artifical Neural Network

Artificial Neural Network (ANN) is a calculation model based on the structure and functions of biological neural networks. ANN can model high-order nonlinear systems where the relationship between variables is unknown or very complex. [27]. ANN has been used in many applications such as pattern recognition, classification, modeling and multivariate data analysis.

An ANN is a network consisting of basic processing units (named nodes or neurons) which can operate in parallel. These structures are influenced by biological neurons in the human brain [28]. The neurons in the neural network are connected by links and each link has a numerical weight associated with it. Each neuron receives input signals through its connections, and it generates a single output signal. Neurons typically implements a non-linear conversion, called the activation function, to the net input to determine the output signal through the outgoing connection of the neuron. [29]. The basic function of elements of a neuron is illustrated in Figure 2.14. Each neuron has an activation (transfer) function. The aim of using activation functions is to limit the input value of a neuron to the desired value range. Each activation function takes a single number and performs a certain constant mathematical operation on it. Various activation functions are available. The most common activation functions are the step, sign, linear and sigmoid functions.

The ANN structure used in this study includes one input layer, two hidden layers and on output layer (4-layered ANN). Logarithmic sigmoid function used as activation function for

hidden layer. The logarithmic sigmoid function transforms the input, which can have any value between positive and negative infinity, to a sensible value between 1 and 0 [29].

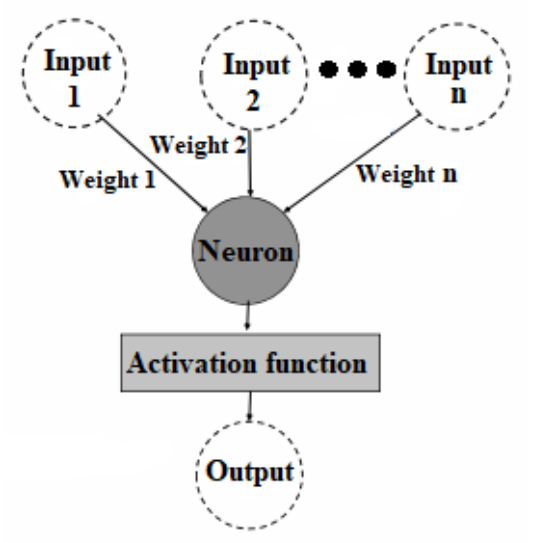

Fig 2.14 The basic function of elements of neuron

The ANN typically consist of three layers: an input layer, a hidden layer and an output layer. These layers can be structured hierarchically. Multilayer network usually contains an input layer, more than one hidden layers, and an output layer. Feedforward network is a network which enables signals to flow only forward direction, from the input to the output layer. As seen in Figure 2.15, a multilayer feedforward neural network has a layered structure.

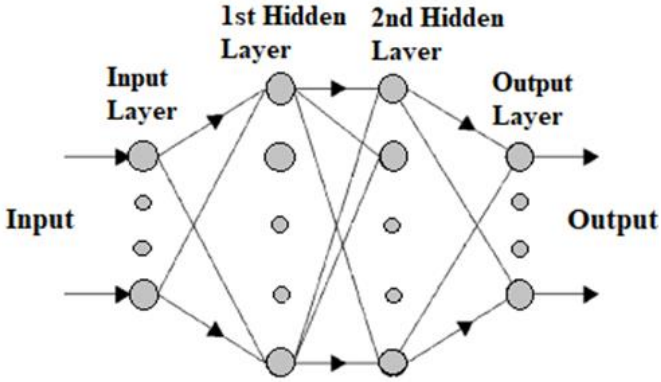

Fig 2.15 Structure of a typical multilayer feedforward neural network

The information flow in ANN starts at the input layer where input data feeds. It does not take place any processing in the input layer. The inputs are weighted and received by neurons in the next layer. Then, the weighted inputs is collected and is activated and generating the output neurons, which are weighted on the processing elements in the next layer, and transmitted. The network alters its weights throughout set of training data and uses a learning

rule until it can find a set of weights that will produce the smallest possible error for input-output mapping. This described process is known as 'training'. In the learning process, training data which is a small subset of the existing dataset to successfully train the network is used. After this, the remaining data can be used to test the network [30].

2.4 Evaluation of Classification Results

To measure the performance of classification applications generally are used sensitivity, specificity and accuracy values. The performance of classification is compared by calculating the accuracy, specificity and sensitivity values of the results of ANN in this study.

The accuracy, sensitivity and specificity values can be calculated using (2), (3) and (4), respectively. Accuracy, sensitivity and specificity are usually showed as a percentage [31].
True Positives (TP): Classification of an unhealthy labeled subject as unhealthy by ANN.
True Negatives (TN): Classification of a healthy labeled subject as a healthy by ANN.
False Positives (FP): Classification of a healthy labeled as unhealthy by ANN.
False Negatives (FN): Classification of an unhealthy labeled as healthy by ANN

The ratio of the number of samples divided into the correct categories is called accuracy. to be unhealthy and healthy to the total number of samples.

$$Accuracy\ (\%) = \frac{\mathrm{TP} + \mathrm{TN}}{\mathrm{TP} + \mathrm{TN} + \mathrm{FP} + \mathrm{FN}} \tag{2}$$

Sensitivity is a probability of a "positive" result when the unhealthy is unhealthy.

$$Sensitivity\ (\%) = \frac{\mathrm{TP}}{\mathrm{TP} + \mathrm{FN}} \tag{3}$$

Specificity is a probability of a "positive" outcome when healthy is healthy.

$$Specificity\ (\%) = \frac{\mathrm{TN}}{\mathrm{TN} + \mathrm{FP}} \tag{4}$$

3. Experiments and Results

3.1 Used Data

The thermal images of premature babies in the Selcuk University, Faculty of Medicine, Neonatal Intensive Care Unit were recorded on the VarioCAM HD infrared camera, the product of InfraTec, which operates in the long wavelength range. The resolution of the camera is 640x480 and thermal sensitivity is about 0.05°C. Thermal images or thermal video sequences are transferred to a computer near the intensive care incubator. Figure 3.1 illustrates how the image acquisition was made. The infrared camera was placed about 60-100 cm away from the neonatal in the supine position. In a 60 second period, 100 frames were captured from neonatal.

Fig 3.1 Thermal image acquisition procedure

Thermograms obtained by using thermal cameras can be converted to temperature maps and color (RGB) images. Color images are produced by converting the thermogram into RGB format between a lower threshold value and an upper threshold temperature value determined by the user by using the thermal image acquisition program. In Figure 3.2 (a), it is displayed an image colored between 30 °C and 40 °C and then converted into a gray-level image. Temperature map represents the matrix of temperature values directly obtained by the thermal camera. The resulting thermogram is recorded in ASCII format without any thresholding. Figure 3.2(b) shows the image produced by visualizing the temperature values. In this study, temperature maps were used.

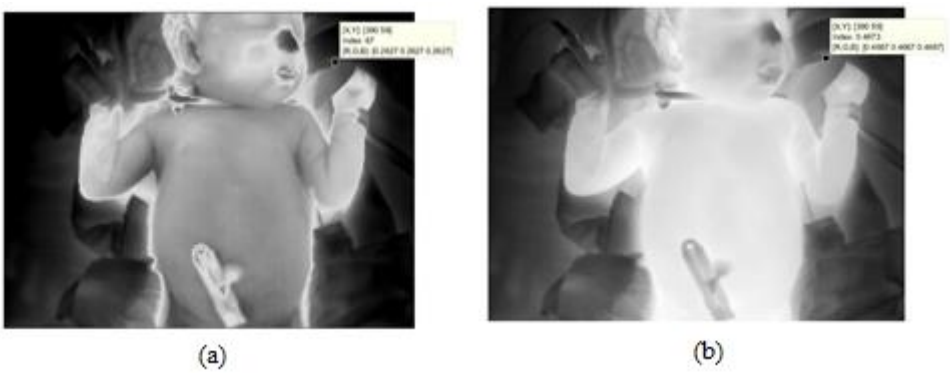

Fig 3.2 Images captured by thermal camera: (a) Gray level of the image captured in the range of 30-40 °C; (b) The image created by visualizing the temperature values

3.2. Experiments

In this study, 190 images belonged to 19 healthy and 19 unhealthy neonates were used. For each neonatal, it was taken 5 images. So, totally 95 healthy-labeled and 95 unhealthy-labeled images were used. This study consists of three steps and these steps were performed in MATLAB platform. The specification of the computer which run the MATLAB: 6 GB DDR3 Memory, Intel i5-2450M CPU (2.5 GHz), 750 GB HDD, and 2 GB NVIDIA GeForce GT 630M GPU.

Firstly, the segmentation process was applied to extract the background from the thermal images. Then, the thermal images with original dimensions of 479 × 640 are set to dimensions of 512 × 512 for use in multiresolution analysis. Although this process caused some pixels to lose, this condition did not affect the analyze because these pixels were outside the region of the body of the neonates.

Secondly, the multiresolution analysis techniques (Wavelet, Curvelet and Contourlet) were used for extracting features of thermal images. Thermal images were divided into approximation and detail coefficients by using multi-resolution analysis methods. The features of thermal images were extracted from the matrix of approximation coefficients. This matrix was normalized in the range [0, 1] and then it was transformed into column vectors to generate feature vectors. Consequently, 190 feature vectors were obtained. For this processes, the optimal decomposition level was determined as 3 for DWT, optimal scale number was specified as 4 for CuT and optimal decomposition level was set to 5 for CoT, empirically. The dimension of the matrix of approximation coefficients was 64x64 for DWT, 85x85 for CuT, and 16x16 for CoT, respectively.

Thirdly, an ANN was used for classification. 190 feature vectors were used as input to the ANN and classification process was conducted. In the ANN, the target of healthy-labeled images was set to 0, and the target of unhealthy-labeled images was set to 1. In the study, the threshold value was determined as 0.5 for healthy-unhealthy classification. Consequently, the result producing from the ANN having a value smaller than 0.5 was labeled as a healthy, and higher than 0.5 and 0.5 was labeled as an unhealthy. The classification process was carried out according to the ten-fold cross-validation test that individually tests each image. According to this test, the entire dataset is firstly divided into 10 equal sets of data. Then, 9 of these 10 sets are used for network training, and the remaining set is used for test network. When the test finishes, the set used in the test is given to the set of training, and a set from the training set is added to the set of test. When this process is repeated 10 times, all the data in the dataset are used to train and test the network. The average of the 10 values obtained as a result of the 10-fold cross validation test will be the estimated value of the established model. Accuracy, sensitivity and specificity rates were calculated to evaluate the results of the ANN. The proposed system diagram is given in Figure 3.3.

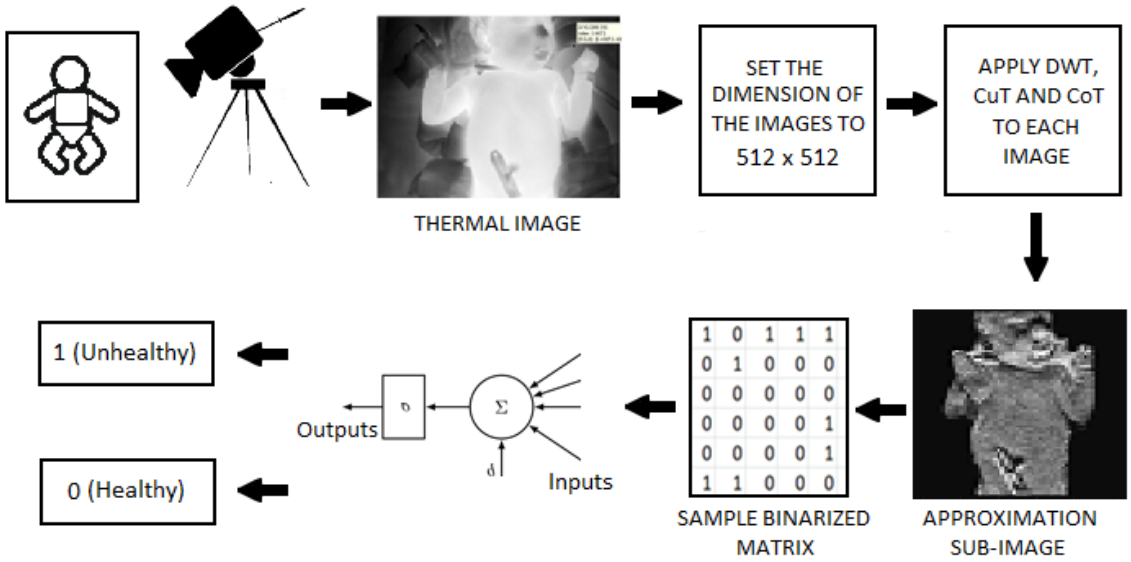

Fig 3.3 Block representation of the proposed system

The structure belonging to ANN used in the study is a four-layered (input layer, 2 hidden layers and output layer), feed-forward and backpropagated. The logarithmic sigmoid function was used as an activation function for two hidden layers. In the ANN model, Gradient descent with momentum was chosen as the training algorithm. The neuron numbers in the hidden layers are 50 and 10, respectively. The appropriate iteration number is determined as 1000 and the learning rate is found 0.04, experimentally.

3.3 Results

In the proposed system, 190 thermal images taken from the neonatal intensive care unit were used. The features of the images were extracted by using three different multiple resolution analysis methods (DWT, CuT and CoT) and the classification was performed by utilizing the ANN model. A 10-fold cross validation method was applied to prove classification validity. The accuracy, sensitivity and specificity values were used to evaluate classification performance.

All numerical results obtained as a result of classification are given in Table 1. As can be seen from Table 1, the highest accuracy rate for classification (98.42%), the highest sensitivity value (100%), and the highest specificity value (96.84%) were achieved by using DWT+ANN. While the accuracy of classification was over 90% for 2D-DWT+ANN and 2D-CuT+ANN, it was 75.26% when 2D-CoT+ANN was used. The result of the experimental study shows that the success of the traditional wavelet transform was superior to the success of the curvelet transform and contourlet transform.

Table 1. Obtained classification results

Method	Accuracy (%)	Sensitivity (%)	Specificity (%)
2D-DWT+ANN	**98.42 (187/190)**	**100 (95/95)**	**96.84 (92/95)**
2D-CuT+ANN	94.21 (179/190)	92.63 (88/95)	95.79 (91/95)
2D-CoT+ANN	75.26 (143/190)	76.84 (73/95)	73.68 (70/95)

Table 2, Table 3 and Table 4 show the TP, TN, FP and FN values obtained according to the result of the classification process. When these tables are examined, it can be seen that for the DWT, the whole of 95 unhealthy-labeled images was classified as an unhealthy. Also, while 92 of 95 healthy-labeled images were classified as a healthy. For CuT, while 88 of 95 unhealthy-labeled images were classified as an unhealthy, 91 of 95 healthy-labeled images were classified as a healthy. For CoD, 73 of 95 unhealthy-labeled images were classified as an unhealthy whereas 70 of 95 healthy-labeled images were classified as a healthy.

Table 2. Obtained result of the classification process for DWT + ANN

		Proposed System Output	
		Positive (Unhealthy)	Negative (Healthy)
Real Label	Positive (Unhealthy)	95	0
	Negative (Healthy)	3	92

Table 3. Obtained result of the classification process for CuT + ANN

		Proposed System Output	
		Positive (Unhealthy)	Negative (Healthy)
Real Label	Positive (Unhealthy)	88	7
	Negative (Healthy)	4	91

Table 4. Obtained result of the classification process for CoT + ANN

		Proposed System Output	
		Positive (Unhealthy)	Negative (Healthy)
Real Label	Positive (Unhealthy)	73	22
	Negative (Healthy)	25	70

Conclusion

Thermal imaging which is used to analyze physiological functions related to skin temperature is a non-invasive, non-ionic and non-contact method. Because of these important characteristics of the thermal imaging, using it in neonatal intensive care units is becoming quite important.

Table 5. The performance comparison of this study with the previous studies

Author	Study design	Field of study	Number of Image	Key findings	Segmentation	Classification	MRA
Anderson et al[32] (1990)	Use of thermographic imaging to study babies sleeping at home	Examining how thermoregulation is achieved by comparing measurements of body temperature and thermographic images of two babies who maintained almost identical rectal temperature patterns in different thermal environments.	5 infants	The skin temperature of sleeping infants was measured and significant heat loss in the head and hands during sleep.	Yes	No	No
Abbas et al[33] (2008)	Neonatal IR-Thermography Pattern Clustering based on ICA Algorithm	Classifying thermal pattern of neonates skin based on ICA mixture model algorithm	12 images	The sensitivity to temperature variation was observed in the head region.	Yes	Using by ICA mixture model learning	Thermal image coefficients were computed and extracted using wavelets algorithm.
Catalan L.B[34] (2009)	Neonatal Infrared Thermography Image Processing	Monitoring the temperature actively by extracting temperature information of ROI which was selected from neonatal	-	-	No	No	No
Rice et al.[35] (2010)	Abdominal Infrared Thermal Imaging for low birth weight infants	Investigating the relationship between the skin temperature of infants with low birth weight and NEC disease.	13 infants	Infants with radiographic NEC had lower abdominal temperature than those without disease ($p < 0,05$ via paired Student's t - test)	No	No	No
Abbas et al[36] (2011)	Neonatal non-contact respiratory monitoring based on real-time infrared thermography	Developing a new non-contact respiration monitoring modality for neonatal intensive care unit using infrared thermography imaging.	7 premature infants	Respiration was detected by **0.3 ºC** and **0.5 ºC** temperature differences.	No	No	Continuous wavelet transformation based on Debauches wavelet function was applied to detect the signal

Abbas et al[10] (2012)	Neonatal infrared thermography imaging: Analysis of heat flux during different clinical scenarios	Testing the accuracy and reliability of thermal imaging under different clinical scenarios (Convective neonatal incubator, kangaroo mother care and Open radiant warmer)	12 preterm infants	In spite of variable tolerance values, the satisfactory results were obtained.	No	No	No
Silva et al[37] (2012)	Early assessment of the efficacy of digital infrared thermal imaging in pediatric extremity trauma	Evaluation of the effectiveness of infrared thermal images in pediatric extremity trauma.	51 children	Infrared thermal images matched 73% of the pain areas. The fractures were seen in 11 patients. Infrared thermal images were matched with 64% fracture sites.	No	No	No
Frize et al[38] (2013)	Infrared Imaging and Classification of Neonates with Necrotising Enterocolitis	A thermal imaging system to detect infants with NEC disease.	20 normal infants and 9 infants diagnosed with NEC	The classification performance of temperature difference between the Upper and the Lower abdomen regions is the highest. **Specificity=90%+/-12%** **Sensitivity=78%+/-18%**	Yes	A Decision Tree classifier was used with 5x5 cross validation	No
Heimann et al[39] (2013)	Infrared thermography for detailed registration of thermoregulation in premature infants.	Evaluating skin temperature by using different positions with non-contact infrared thermography in multiple body areas of preterm infants.	10 premature infants	Infrared thermography showed significant increase in head and leg skin temperature, following 90 minutes of neonatal skin-to-skin care ($p<0.05$)	No	No	No
Abbas et al[40] (2014)	Intelligent neonatal monitoring based on a virtual thermal sensor	Tracking different geometric profiles and shapes over the external anatomy of a neonate accurately via virtual temperature sensing application.	10 neonates	The range of **ROI** tracking success rate was between **74% and 89%** ($p<0.01$)	No	No	No
This study	Classification of unhealthy and healthy neonates in neonatal intensive care units using medical thermography processing	Multi-resolution analysis and artificial neural network were used to make healthy – unhealthy classification of newborn intensive care units infants.	190 images from 38 neonates	**Accuracy: 98.42%, Sensitivity 100%, Specificity: 96.84%** when using 2D-DWT+ANN	Yes	ANN	Yes

In this study, 190 images belonged to 19 healthy and 19 unhealthy neonates were used to classify these neonates as a healthy or unhealthy. The result of the classification shows that if thermal imaging is used with machine learning together, it will be possible to achieve an important breakthrough in the medical field. For example, a pre-diagnosis system which detects diseases early can be designed by combining these two techniques.

As shown in Table 5, this study yielded more successful results by combining multiresolution analysis with artificial neural networks, as compared to studies in the literature. Also, the high number of data used ensures consistency in the study results. Very few of the studies done in the literature have been a segmentation process and therefore our work stands out.

In the future, it can be developed a pre-diagnosis system which based on thermal imaging to analyze a region in the body of neonates which marked by the specialist without causing any disturbance and radiation damage to neonates. Developing this system can be very important concerning two points. Firstly, the diseases of neonates that are observed in the neonatal intensive care unit can be detected early and this may result in reducing the mortality for neonates. Secondly, preterm neonates and low birthweight infant can be monitored for 24 hours and the body parts of them can be analyzed to inform doctors about their health status.

ACKNOWLEDGMENT

This study was supported by the Scientific and Technological Research Council of Turkey (TUBITAK, project number: 215E019).

REFERENCES

[1] Rogalski A, Chrzanowski K (2012) Infrared devices and techniques. Opto-Electronics Review 10:2:111–136

[2] Sruthi S, Sasikala M (2015) A low cost thermal imaging system for medical diagnostic applications. International Conference on Smart Technologies and Management for Computing, Communication, Controls, Energy and Materials (ICSTM), 621–623

[3] Bouzida N, Bendada A, Maldague X.P (2009) Visualization of body thermoregulation by infrared imaging. Journal of Thermal Biology 34:120–126

[4] Ring E.F.J, Ammer K (2012) Infrared thermal imaging in medicine. Physiological Measurement 33:33-46

[5] Lahiri B.B, Bagavathiappan S, Jayakumar T, Philip J (2012) Medical applications of infrared thermography: A review. Infrared Physics&Technology 55: 221–235

[6] Jones B.F (1998) A reappraisal of the use of infrared thermal image analysis in medicine. IEEE Transactions on Medical Imaging 17:6:1019–1027

[7] Hildebrandt C, Zeilberger K, Ring E.F.C, Raschner C (2012) The application of medical infrared thermography in sports medicine. An International Perspective on Topics in Sports Medicine and Sports Injury 14:258–274

[8] Knobel R.B, Guenther B.D, Rice H.E (2011) Thermoregulation and thermography in neonatal physiology and disease, Biological Research for Nursing, 13:3:274–282

[9] Govindarajan J (2007) A Case for joint development of Ir cameras in India. Journal on Intelligent Electronic Systems 1:1:26-27

[10] Abbas K, Heimann K, Blazek V, Orlikowsky T, Leonhardt S (2012) Neonatal infrared thermography imaging: Analysis of heat flux during different clinical scenarios. Infrared Physics & Technology 55:538–548

[11] Morlet J, Arehs G, Forugeau I, Giard D (1982) Wave propogation and sampling theory. Geophysics, 47:2:203–236

[12] Mallat S (1989) A theory for multiresolution signal decomposition: The wavelet representation. IEEE Transactions on Pattern Analysis and Machine Intelligence 11:7:674–693

[13] Daubechies I (1992) Ten lectures on wavelets. CBMS-NSF Regional Conference Series in Applied Mathematics, Philadelphia, 53-105

[14] Kulkarni1 S.M, Shelke A.R (2014) Multiresolution analysis for medical image segmentation using wavelet transform. International Journal of Emerging Technology and Advanced Engineering (IJETAE) 4:6:543–545

[15] Fadili J.M, Starck J.L (2009) Curvelets and ridgelets. R.A. Meyers, ed. Encyclopedia of Complexity and Systems Science, 14, Springer New York, 1718-1738

[16] Candes E.J, Donoho D.L (2000) Curves and surface fitting (Curvelets-A surprisingly effective nonadaptie representation for objects with edges). Vanderbilt University Press, Nashville, 105–120

[17] Do M.N, Vetterli M (2005) The contourlet transform: An efficient directional multiresolution image representation. IEEE Transactions on Image Processing 14:12:2091 – 2106

[18] Rioul O, Vetterli M (1991) Wavelets and signal processing. IEEE Sig. Proc. Mag, 14 – 38

[19] Ervural S, Ceylan M (2015) Determination of benign and malign lesions by fusion of the different phases of liver MR. 25th Signal Processing and Communications Applications Conference (SIU), 1–4

[20] Alzubi S, İslam N, Abbod M (2011) Multi-resolution analysis using curvelet and wavelet transforms for medical imaging. Medical Measurements and Applications Proceedings, 188–191

[21] Ceylan M (2009) A new complex-valued intelligent system design on evaluating of the lung images with computerized tomography, PhD Thesis, The graduate school of natural and applied science of Selcuk University, Konya, Turkey, 21–50

[22] Candes E.J, Donoho D.L (2004) New tight frames of curvelets and optimal representations of objects with piecewise C2 singularities. Communications on Pure and Applied Mathematics: A Journal Issued by the Courant Institute of Mathematical Sciences, 57:2:219–266

[23] Donoho D.L, Duncan M (1999) Digital curvelet transform strategy. Implementation and Experiments, Department of Statistics Stanford University

[24] Candes E.J, Guo F (2002) New multiscale transforms, minimum total variation synthesis: Application to edge-preserving image reconstruction. Signal Processing 82:11:1519–1543

[25] Candes E.J, Demanet L, Donoho D.L, Ying L (2006) Fast discrete curvelet transforms. Multiscale Modeling and Simulation 5:3:861–899

[26] Toro-Garay G.H, Medina-Daza R.J (2017) Fusion of worldview2 images using contourlet, curvelet and ridgelet transforms for edge enhancement. Revista Facultad de Ingeniería 85:8–17

[27] Amato F, López A, Peña-Méndez E.M, Vaňhara P, Hampl A, Havel J (2013) Artificial neural networks in medical diagnosis. Journal of Applied Biomedicine 11: 47–58

[28] Basheer I, Hajmeer M (2000) Artificial neural networks: Fundamentals, computing, design, and application. J Microbiol Meth 43: 3–31

[29] Negnevitsky M (2005) Artificial Intelligence. A Guide to Intelligent Systems, Second Edition.

[30] Freeman J.A, Skapura D.M (1991) Neural Networks Algorithms, Applications, and Programming Techniques. Computation And Neural Systems Series, Series Editor

[31] Sharma D, Yadav U.B, Sharma P (2009) The concept of sensitivity and specificity in relation to two types of errors and its application in medical research. Journal of Reliability and Statistical Studies 2: 53–58

[32] Anderson E.S., Wailoo M.P., Petersen SA (1990) Use of thermographic imaging to study babies sleeping at home. Archives of Disease in Childhood: Short reports, 65:1266–1267

[33] Abbas A.K., Leonhardt S (2008) Neonatal IR-Thermography pattern clustering based on ICA Algorithm. Color Image processing workshop, Aachen

[34] Catalan L.B. (2009) Neonatal infrared thermography image processing. Aachen University:Msc. Thesis

[35] Rice H.E, Hollingsworth C.L, Bradsher E, Danko M.E, Crosby S, Goldberg R.N, Tanaka D.T, Knobel R.B (2010) Infrared thermal ımaging (thermography) of the abdomen in extremely low birthweight infants. The Journal of Surgical Radiology, 1:2:82-89

[36] Abbas A.K, Heimann K, Jergus K, Orlikowsky T, Leonhardt S (2011) Neonatal non-contact respiratory monitoring based on real-time infrared thermography. BioMedical Engineering OnLine,10:93

[37] Silva C.T, Naveed N, Bokhari S, Baker K.E, Staib L.H, İbrahim S.M, Muchantef K, Goodman T.R (2012) Early assessment of the efficacy of digital infrared thermal imaging in pediatric extremity trauma. Emerg. Radiol., 19:203-209

[38] M. Frize, R. Nur, E. Bariciak and C. Herry (2013) Infrared imaging and classification of neonates with Necrotising Enterocolitis. In World Congress on Medical Physics and Biomedical Engineering 2012, Beijing, China, Springer, Berlin, Heidelberg, pp 1309-1312

[39] Heimann K, Jergus K, Abbas AK, Heussen N, Leonhardt S, Orlikowsky T (2013) Infrared thermography for detailed registration of thermoregulation in premature infants. J Perinat Med, 41:5:613–620

[40] Abbas AK, Leonhardt S (2014) Intelligent neonatal monitoring based on a virtual thermal sensor. BMC Medical Imaging, 14:9